EVAPORATOR OPTIMIZATION FOR NON-UNIFORM AIR DISTRIBUTION

Piotr A. Domanski[a], David A. Yashar[b], and Sunil Lee[c]
HVAC&R Equipment Performance Group
National Institute of Standards and Technology
Gaithersburg, MD 20899-8631, USA
[a]piotr.domanski@nist.gov; [b]david.yashar@nist.gov; [c]sunil.lee@nist.gov

ABSTRACT

This study demonstrates the performance improvements that can be achieved by accounting for the air flow distribution during the design phase of a heat exchanger. The heat exchanger used in this study was a two-slab, A-shaped finned-tube evaporator installed in a horizontal duct with a condensate collection pan and condensate droplet collection metal sheet. The installation configuration and attachments resulted in a large degree of air maldistribution, with approximately 20 % more air passing through the upper slab than the lower slab. Additionally, the heat exchanger's mounting brackets blocked air flow to the refrigerant tubes closest to the front edge of the slabs resulting in minimal air flow to these tubes.

In this analytical effort, we used the NIST heat exchanger model EVAP-COND and Intelligent System for Heat Exchanger Design (ISHED) to examine options for improving the evaporator design for its capacity with the actual, measured air velocity profile. Optimization of the refrigerant flow split between the two slabs provided 1.1 % capacity improvement, while optimization of refrigerant circuitry for both slabs improved the capacity by 5.6 %. Simulations also showed that the tubes with minimal air flow had a very small contribution to the overall capacity, and that eliminating them from the assembly may prove to be an attractive cost saving method. Evaporator designs with optimized refrigerant circuitry and reduced number of tubes had better capacities than the original 120-tube evaporator, showing an improvement of 5.2 % for a 108-tube design and 4.0 % for a 102-tube design.

1. INTRODUCTION

The effect of inlet air distribution on the performance of refrigerant-to-air heat exchangers can be substantial. Several capacity degradation cases are documented in the literature, e.g., Fagan (1980) reported a capacity reduction as much as 20 % for maldistribution exceeding 50 % of the average coil velocity, and Chwalowski et al. (1989) measured degraded capacity by as much as 30 % for air-conditioning evaporators. Nevertheless, the prevailing heat exchanger design practice today does not account for air distribution but may implement a refrigerant circuitry that could offer some degree of robustness with a non-uniform air velocity profile. This practice is a consequence of (1) the difficulty in determining the air distribution at the inlet to a heat exchanger as installed and (2) the lack of effective guidelines and tools for designing an optimized heat exchanger for the actual air flow distribution.

This paper presents an optimization case study for a two-slab, A-shape evaporator. We used the information on inlet air distribution that Yashar and Domanski (2009) obtained through particle image velocimetry (PIV) measurements and computational fluid dynamics (CFD) simulations. Our effort was concerned with the optimization of refrigerant circuitry to accommodate the measured inlet air distribution. We also examined the option of removing several individual tubes that were deemed ineffective. We determined the benefits of the optimized designs using NIST's EVAP-COND heat exchanger simulation model (Domanski, 2008).

2. OPTIMIZATION OF REFRIGERANT CIRCUIRTY

Several researchers have indicated the importance of proper refrigerant circuitry design in finned-tube heat exchangers. Liang at al. (2001) concluded that a 5 % savings in the heat transfer area is possible with proper refrigerant circuit design. Casson et al. (2002) presented simulation results indicating the benefits of high-mass-flux circuitry designs for high-pressure refrigerants. Granryd and Palm (2003) performed an analytical study in which they linked the optimal heat exchanger operation to the relationship between the drop of refrigerant saturation temperature and the average temperature difference between the refrigerant and the tube wall.

In previous studies, we have used the evolutionary computation-based Intelligent System for Heat Exchanger Design (ISHED) (Domanski et al., 2004) to optimize the sequence of connections between all existing tubes in the heat exchanger assembly. ISHED consists of the heat exchanger simulator EVAP-COND, which provides capacities of heat exchangers with different circuitry designs, and a set of modules that generate new circuitry architectures. Experimentation for optimizing performance of evaporators (Domanski et al., 2005) and condensers (Domanski and Yashar, 2007) with non-uniform air velocity profiles showed that ISHED-generated circuitry designs are as good as or better than circuitry prepared manually.

2. HEAT EXCHANGER STUDIED

The heat exchanger used in the present study was a 10.5 kW residential air-conditioning, finned-tube heat exchanger shown in Figure 1. It consisted of two identical slabs configured in an A-shape with an apex angle of 40 degrees. Each slab had three tube depth rows with 20 tubes per row and wavy fins. The tubes were micro-finned inside, had an outside diameter of 9.5 mm, and were assembled in a staggered tube configuration.   The tubes were spaced 25.4 mm apart, and the depth rows were spaced 19 mm apart. The overall dimensions of each slab were: a width of 508 mm, a length of 457 mm, and a thickness of 57.2 mm. The heat exchanger assembly was installed in the horizontal duct, with a condensation collection device comprised of a plastic tray at the base of the heat exchanger and a condensate trapping metal sheet.

It is important to note the plastic mounting bracket attached to the base of the test coil. This bracket was necessary to hold the coil position in the duct and maintain the angle between the two slabs. The bracket could also act as a condensation runoff conduit if the coil were positioned in the up flow configuration with the base positioned at the bottom and the apex at the top. The mounting bracket overlapped a 45 mm wide strip of the inlet surface of both slabs, indicated by the ellipse in Figure 1, effectively sealing off this area for air flow.
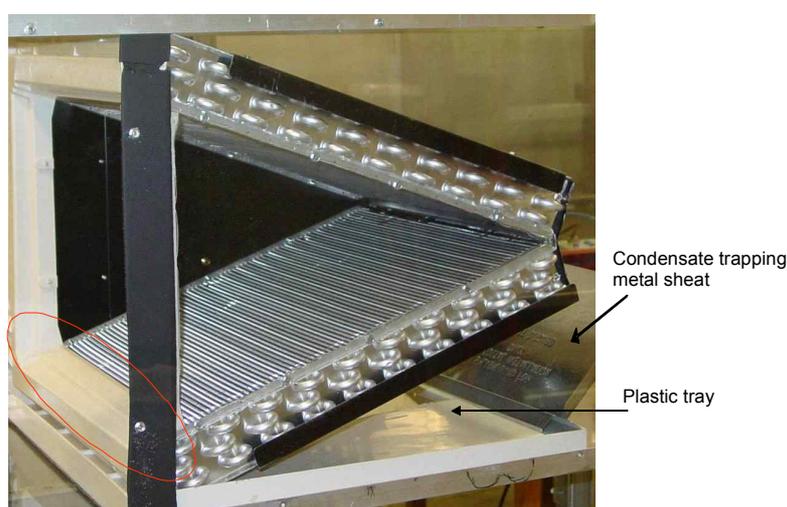
Figure 1. Test coil with emphasis on inner lip of mounting bracket

3. AIR FLOW DISTRIBUTION

3.1 Test Apparatus and Measurement Methods

The test apparatus was housed in an environmental chamber and consisted of three components: a chilled water flow loop, an air flow loop, and a PIV air flow measurement system. The air flow loop consisted of the test section, air flow measurement section, and control section. The test section was a plexiglass duct constructed around the test coil. In the measurement and control section, the air flowed through a nozzle, and then through a blower powered by a variable-speed motor. The flow rate was measured according to ASHRAE Standard 37 (1998).

The PIV measurement system consisted of a pair of Class IV pulsed lasers outfitted with a sheet forming optical lens, a double framed Charged Coupled Device camera, a theater-style fog generator, and a Programmable Timing Unit (PTU) controlled by a computer. PIV works on the principle of tracking the motion of ''seed'' particles entrained in the flow field. The seed particles act as markers within the flow field whose displacement is mapped between two points in time. A series of laser light sheets illuminates the seed particles as they move through the test section. A camera captures images of the particles and therefore records the distance traveled by the particles over a fixed length of time, which allows us to extract the velocity. Detailed information on the test apparatus and measurement methods are reported in Yashar and Domanski (2009).

3.2 Measurement and Simulation Results

In this study, we used the measured inlet air flow velocity profiles shown in Figure 2, denoted as Test 1 in Yashar and Domanski (2009). The plotted data are the PIV measurement points for the approach air flow to the upper and lower slabs; they are the components of the velocity vectors perpendicular to the surface of the coil. The horizontal axis shows the position along the slabs, with zero being the inlet of the coil and 508 mm at the apex. The data for both slabs show similar patterns. First, the bottom most 50 mm – 60 mm of the heat exchanger receives no air flow because the mounting bracket blocks this portion of the heat exchanger's inlet surface. At a certain point afterwards, there is a spike of the air flow incident on the coil; this region is shown at approximately 65 mm – 100 mm on the figure. It is also of interest to note the rapid decrease in air flow near the apex.

The measurements indicated that there was a significant difference in the amount of air flowing through the two slabs. Numerical integration of the PIV data showed that 17.9 % more air passed through the upper slab than the lower one. The presence of the condensation collection device effectively increased the resistance for the air passing through the lower slab; therefore, some air flow was routed away from the lower portion of the test section and passed through the upper slab.
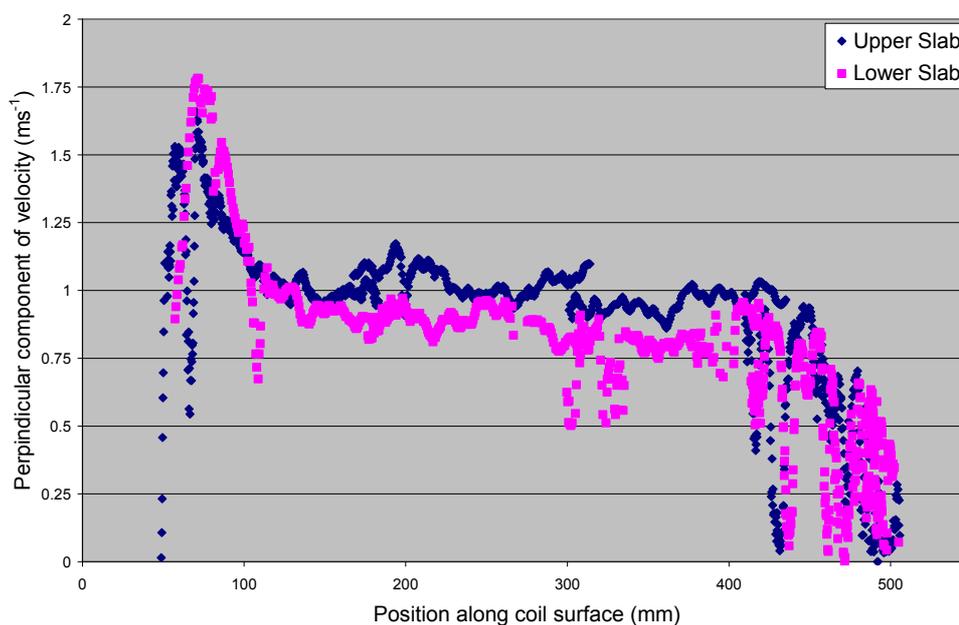
Figure 2. Inlet air velocity profiles for upper and lower slabs (Test 1, Yashar and Domanski, 2009)

In addition to the PIV measurements, a CFD-based model of the heat exchanger was constructed through a momentum resistance modeling approach. The CFD simulation results for a location 10 mm upstream of the coil agreed with the measurement data to within ±15 % for 93 % of the span of the coil.

Since the simulation results for both heat exchanger slabs agreed fairly well with the measured data at the air inlets and exits, we can assume that the CFD solution of the air flow inside the coil is reasonably accurate. This information is very interesting because it is a key factor for determining the air-side heat transfer coefficients. Figure 3 shows a map of the velocity magnitude (combined parallel and perpendicular components) overlaid with an array of circles representing the placement of tubes in the heat exchanger. This figure shows that eight tubes in the lower slab and four tubes in the upper slab were exposed to air velocities below 0.4 ms^{-1}. These tubes are therefore incapable of transferring a significant amount of heat and will underperform compared to the other tubes in the coil.
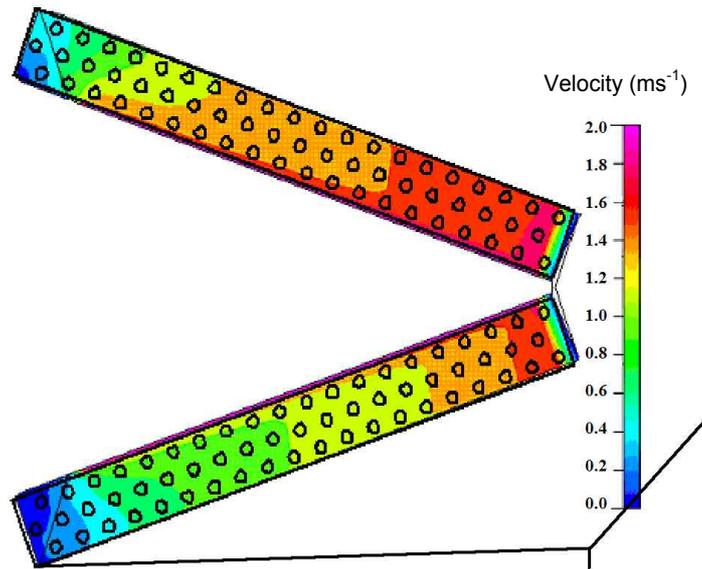
Figure 3. Map of velocity magnitude (Test 1, Yashar and Domanski, 2009)

4. OPTIMIZATION CASES

We varied a number of selected parameters to determine their impacts on the heat exchanger performance. We performed all the simulations using the EVAP-COND simulation model, which has been validated against various experimental data sets (e.g., Payne and Domanski, 2003) and has proven to be a very effective tool in several system and heat exchanger sensitivity studies. Throughout this study, the design parameters related to the manufacturing process, such as tube diameters, tube and depth row spacing, fin spacing, etc., were not modified from the original design. Also constant were the following heat exchanger operational parameters:
  - Inlet air condition: 26.6 °C dry-bulb temperature, 50 % relative humidity, 101.325 kPa pressure
  - Total air volumetric flow rate: 0.567 m^{3}s^{-1}
  - Inlet refrigerant quality: 0.20
  - Refrigerant saturation temperature at the heat exchanger assembly exit: 7.2 °C
  - Refrigerant superheat at the heat exchanger assembly exit: 5.6 °C

Table 1 presents the seven cases studied. The varied parameters include the inlet air velocity profile, air split between the upper and lower slabs, refrigerant flow split between the upper and lower slabs, refrigerant circuitry design, and the number of tubes in the heat exchanger.

The starting point, Case 1, considered the original refrigerant circuitry design for the test coil with idealized operating conditions. The total air flow was divided equally between the two slabs, and its velocity profile was uniform. The refrigerant split between the two slabs was also equal, which probably was the case during the tests because of the equal flow restrictions of the lines that distributed refrigerant to the slabs.

In Case 2, we used all of the Case 1 parameters except the even air flow split between the two slabs. In particular, we assigned 55 % of the total air flow to go through the upper slab and 45 % of the air to go through the lower slab (i.e., the upper slab had a 22.2 % higher air flow rate than the lower slab). This air flow split approximated the measured split, which was affected by the flow resistance imposed on the lower part of the coil assembly by the condensate trapping metal sheet.

We denoted Case 3 as the *Reference case* because the parameters for Case 3 closely approximates the conditions of the laboratory tests of the A-shape assembly. Here, we incorporated the non-uniform air velocity profiles presented in Figure 4. These profiles approximate the PIV measurements shown in Figure 2 since the simulation model EVAP-COND could not accept the detail and amount of data rendered with the PIV measurements. However, the air velocity profiles implemented represent the most important features of the measured velocity profile, i.e., the minimal amount of air flow at the inlet to the heat exchanger assembly and the gradual reduction in the air flow at the apex. Following the measured data, the upper and lower slab velocity profiles are different. We also divided the refrigerant flow evenly between each slab since the original coil had an equivalent set of distributor tubes feeding refrigerant to each slab.

Cases 4 through 7 introduce some optimization aspects, one parameter at a time. A newly introduced parameter, compared to the preceding one, is marked for each case in Table 1 by a shaded area. For all these cases, we used the 0.55/0.45 air split and the same non-uniform velocity profiles as for the reference Case 3.
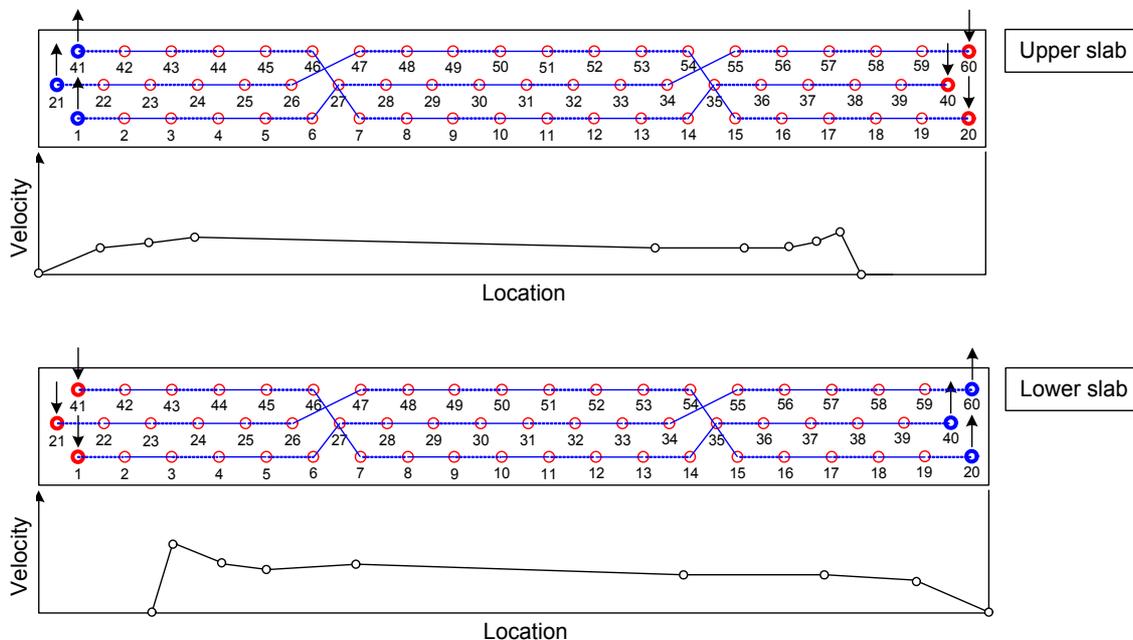
Figure 4. EVAP-COND representation of the original refrigerant circuitry for the lower and upper slabs and the corresponding inlet air velovity profiles (Case 3)

In Cases 1, 2 and 3, refrigerant superheats at the individual slab exits were not controlled; however, the target 5.6 °C superheat at the exit of the heat exchanger assembly was obtained by mixing the two unevenly superheated refrigerant streams exiting each slab. The exit superheat was particularly unbalanced for Cases 2 and 3, where we introduced the uneven 0.55/0.45 split of air flow. This unbalanced air flow caused the refrigerant exiting the upper slab to have a higher level of superheat than the refrigerant exiting the lower slab. Starting with Case 4, we controlled the refrigerant flow rate in each slab to ensure that the refrigerant superheat at the exit of the individual slabs were the same and equaled the target superheat of 5.6 °C. In practice, this would be accomplished by modifying the distributor that feeds refrigerant to the slabs.

Table 1. Varied parameters of the cases studied

Varied Parameters		Case 1	Case 2	Case 3	Case 4	Case 5	Case 6	Case 7
		← *Idealized*		*Reference*	*Optimized* →			
Air flow split (fraction)	Upper slab	0.50	0.55	0.55	0.55	0.55	0.55	0.55
	Lower slab	0.50	0.45	0.45	0.45	0.45	0.45	0.45
Air velocity profile		uniform	uniform	non-uniform	non-uniform	non-uniform	non-uniform	non-uniform
Refrigerant flow split (fraction)	Upper slab	0.50	0.50	0.50	0.54	0.54	0.54	0.54
	Lower slab	0.50	0.50	0.50	0.46	0.46	0.46	0.46
Refrigerant circuitry		original	original	original	original	optimized	optimized	optimized
Number of tubes in a row per slab		20/20/20	20/20/20	20/20/20	20/20/20	20/20/20	18/18/18	17/17/17

Table 2. Predicted heat exchanger performance

Performance		Case 1	Case 2	Case 3	Case 4	Case 5	Case 6	Case 7
		← *Idealized*		*Reference*	*Optimized* →			
Capacity	Upper slab	7.033	7.155	6.920	7.306	7.584	7.551	7.487
	Lower slab	7.010	6.709	6.495	6.274	6.580	6.565	6.465
	Total	14.043	13.864	13.415	13.580	14.164	14.116	13.952
	Referenced to Case 3	**1.047**	**1.034**	**1.000**	**1.012**	**1.056**	**1.052**	**1.040**
Refrigerant exit superheat	Upper slab	5.8	9.8	9.7	5.6	5.6	5.6	5.6
	Lower slab	5.3	1.4	1.8	5.6	5.6	5.6	5.6

The new element introduced in Case 5 is the refrigerant circuitry which was optimized for the given set of operating conditions. Figure 5 shows the ISHED-generated circuitry designs after we modified them manually to account for various manufacturing constraints.
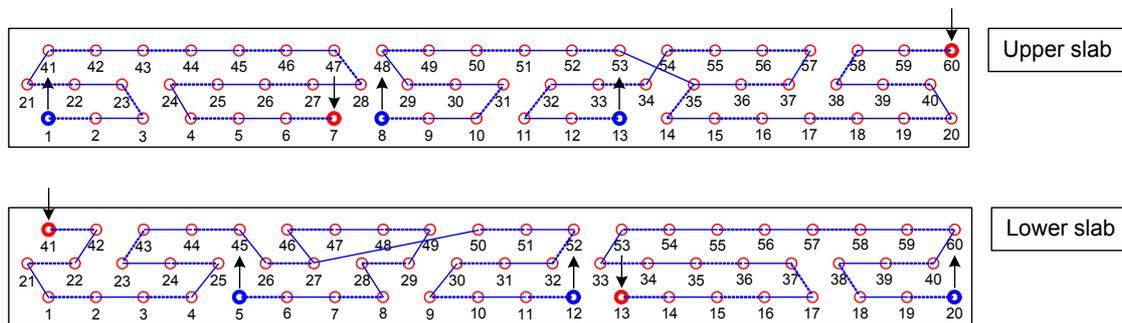
Figure 5. EVAP-COND representation of the refrigerant circuitry for the upper and lower slabs optmized by ISHED for the non-uniform air velocity profile (Case 5)

In Cases 6 and 7, we removed some of the air-starved tubes from the entry areas of both slabs, which were covered by the mounting bracket. In Case 6, we removed a total of 12 tubes, two tubes per depth row in both slabs, which left 108 tubes in the assembly. With reference to Figure 4, Case 6 involved removing tubes 19, 20, 39, 40, 59 and 60 for the upper slab, and tubes 1, 2, 21, 22, 41, and 42 for the lower slab. In Case 7, we removed 18 tubes, three tubes per depth row, resulting in a 102-tube evaporator. In this case, we additionally removed tubes 18, 39, and 59 from the upper slab and tubes 3, 23, and 43 from the lower slab. The rationale for removing the tubes was the savings of the tube material, 10 % for Case 6 and 15 % for Case 7, respectively. The tube removal made the heat exchange area smaller since the tube spacing remained unchanged. Figure 6 shows the ISHED-generated circuitry designs for Case 6 after we modified them manually to account for various manufacturing constraints.
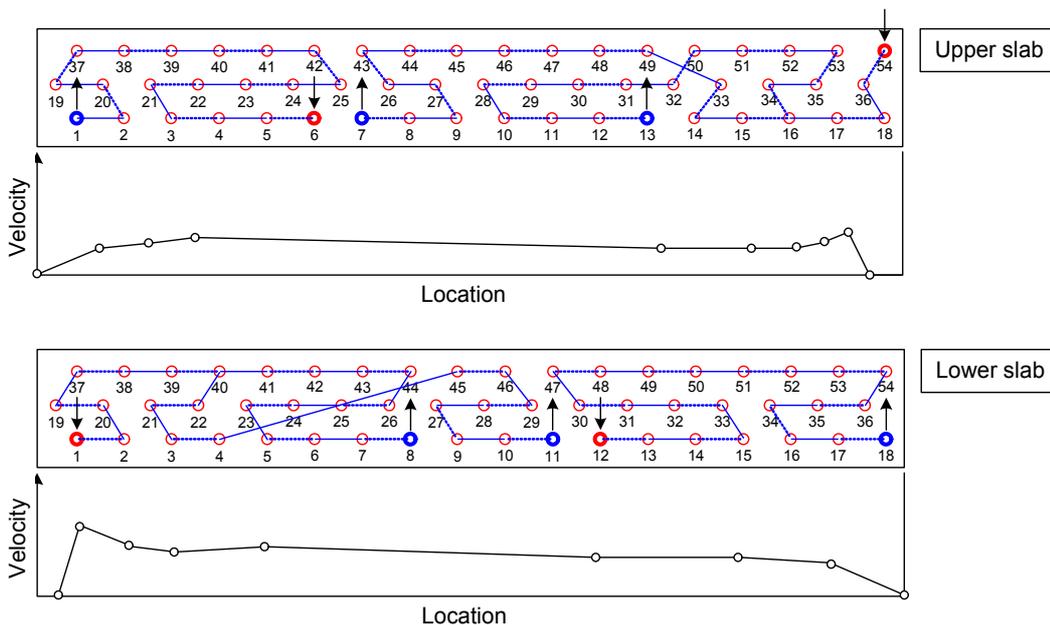
Figure 6. EVAP-COND representation of the ISHED-optimed refrigerant circuitry for the upper and lower slabs with reduced numbers of tubes to 18 per depth row, and the corresponding non-uniform inlet air velocity profiles (Case 6)

Table 2 presents simulation results   Comparing Case 1 to the reference Case 3, the capacity of the heat exchanger can be made to be 4.7 % higher if the air split between the slabs is made equal and the inlet air velocity profile uniform (Case 1). The result for Case 2 indicates that the loss in capacity is more strongly tied to the non-uniform air velocity profile than the uneven air flow split between the slabs.

Advancing the design from Case 3 to Case 4 by optimizing the refrigerant flow split to achieve the same 5.6 °C refrigerant superheat at both slab exits improved the capacity by only 1.2 %.

The highest capacity was achieved by Case 5, which features an ISHED-optimized refrigerant circuitry in addition to an optimized refrigerant flow split. The Case 5 capacity also exceeds the capacity obtained by the original refrigerant circuitry with a uniform air velocity profile and equal air flow split between the slabs (Case 1). Cases 6 and 7 achieved improved capacities, compared to the reference case, by 5.2 % and 4.0 %, respectively, while simultaneously reducing the number of tubes by 10 % and 15 %, respectively, indicating that the selectively removed tubes offered a small contribution to the capacity for the heat exchanger assembly.

5. CONCLUSIONS

This study showed the potential for improving capacity of the studied evaporator by 5.6 % by optimizing the refrigerant circuitry and the refrigerant flow split between the two slabs. Simulations also showed that the tubes with minimal air flow had a very small contribution to the overall capacity, and thus eliminating them from the assembly may prove to be an attractive cost saving method. Evaporator designs with optimized circuitry and reduced numbers of tubes had better capacities than the original 120-tube evaporator, showing an improvement of 5.2 % for a 108-tube design and 4.0 % for a 102-tube design. An experimental verification of the above conclusions will be conducted in the future.

REFERENCES

ASHRAE 1998. ANSI/ASHRAE Standard 37, Methods of Testing for Rating Unitary Air Conditioning and Heat Pump Equipment, *American Society of Heating, Refrigerating and Air-Conditioning Engineers*. Atlanta, GA.

Casson, V., Cavallini, A., Cecchinato, L., Del Col, D., Doretti, L., Fornasieri, E., Rossetto, L., Zilio, C. 2002, Performance of Finned Coil Condensers Optimized for New HFC Refrigerants, *ASHRAE Trans*. 108(2), 517-528.

Chwalowski, M., Didion, D. A., and Domanski, P. A., 1989, Verification of Evaporator Computer Models and Analysis of Performance of an Evaporator Coil, *ASHRAE Trans*. 95(1), 1229-1236.

Domanski, P.A., 2008, EVAP-COND - Simulation models for finned-tube heat exchangers, Version 2.3, National Institute of Standards and Technology, Gaithersburg, MD, USA. http://www2.bfrl.nist.gov/software/evap-cond/.

Domanski, P.A., Yashar, D., 2007, Optimization of Finned-Tube Condensers Using an Intelligent System, *Int. J. Refrig*. 30(4), 482-488.

Domanski, P.A., Yashar, D., Kaufman, KA., Michalski R.S., 2004, Optimized design of finned-tube evaporators using learnable evolution methods, *Int J HVAC&R Research* 10(2), 201-212.

Domanski, P.A., Yashar, D., Kim, M., 2005, Performance of a finned-tube evaporator optimized for different refrigerants and its effect on system efficiency, *Int. J. Refrig*. 28(6), 820-827.

Fagan T.J., 1980, The effects of air flow maldistribution on air-to-refrigerant heat exchanger performance, *ASHRAE Trans*. 86(2), 699-713.

Granryd, E., Palm, B, 2003, Optimum Number of Parallel Sections in Evaporators *Int.Congress Refrig*., Paper ICR0077.

Liang, S.Y., T.N. Wong, G.K. Nathan, 2001, Numerical and experimental studies of refrigerant circuitry of evaporator coils, *Int. J. Refrig*. 24(8), 823-833.

Payne W. V., Domanski, P.A., 2003, Potential Benefits of Smart Refrigerant Distributors, report to Air-Conditioning and Refrigeration Technology Institute, report ARTI-21CR/605-200-50-01. http://www.bfrl.nist.gov/863/HVAC/pubs/PDF/SDR%20Report%20411.pdf

Yashar, D.A., Domanski, P.A., 2009, Particle Image Velocimetry Measurements and CFD-Based Predictions of Air Distribution at Evaporator Inlet and Outlet, ARTI Report No. 07010-01, http://www.ahrinet.org/Content/downloads/research/Research-Final/ARTI-Rpt-07010-01.pdf.